Broadband Printed Tapered Slot Antenna Fed by CPW Fulfilled with Planar Artificial Magnetic Conductor for X-Band Operation

Hossein Malekpoor
Department of Electrical Engineering, Faculty of Engineering, Arak University, Arak, 38156-8-8349, Iran

Corresponding author: Hossein Malekpoor (h-malekpoor@araku.ac.ir).

ABSTRACT A low-profile printed slot antenna (PSA) backed by broadband planar artificial magnetic conductor (AMC) is introduced in this study. Firstly, a suggested PSA with the radiating tapered slots excited by coplanar waveguide (CPW) is used to expand the bandwidth in the measured range of 9-11 GHz ($S_{11} \leq$ -10 dB). Then, the suggested planar AMC surface as the ground plane of the antenna is inserted into the PSA to gain improved radiation efficiency. The realized result from the PSA with the 9×9 planar AMC array exhibits -10 dB measured impedance bandwidth from 6.63 to 13.73 GHz (70%). The suggested PSA with AMC compared to the PSA without AMC exhibits a size reduction of 60%, enhanced bandwidth of 50%, and excellent impedance matching with a minimum value of almost -40 dB. The novel AMC unit cell is realized to operate at 10.14 GHz with an AMC bandwidth of 8-12.35 GHz (43.1%) for X-band operation. Besides, by loading a periodic AMC unit cell into PSA, a high gain of more than 11 dBi with uni-directional radiation patterns is achieved.

INDEX TERMS Artificial Magnetic Conductor (AMC), Printed Slot Antenna, Planar AMC, Wideband AMC.

I. INTRODUCTION

In most studies, electromagnetic band gap (EBG) structures have been employed in many wireless networks and a wide variety of electromagnetic equipment due to the unique and remarkable characteristics. They exclude the surface wave's propagation in a determined frequency gap. The EBG structures are studied and recognized as the photonic band gap (PBG) structures with periodic arrangements [1]-[4]. As is known, the artificial magnetic conductor (AMC) structures introduce a privilege like a perfect magnetic conductor (PMC) with in-phase reflection response entire the certain range. Based on this, multiple low profile antennas and mode prevention designs are applied AMCs as diverse surfaces to augment the distinguishing features [5]-[10]. The results presented in [9] show a broadband patch array by loading diverse EBG-AMCs into the ground plane. Also, a miniaturized uni-planar metamaterial-based EBG for parallel-plate mode prevention of the switching noise in digital circuits is described in [10].

The uses of AMC periodic surfaces in distinct combinations are provided to show better efficiency [11]-[18]. Among these works, a mushroom-shaped AMC structure as a beneficial approach is usually applied for diverse arrangements to achieve the low-profile structures with a higher efficiency [11]. In this method, used vias in periodic arrangements cannot create an easy accomplishment in the printed circuits and devices due to the drilled holes in a substrate. In the recent work, an EBG mushroom surface with a dual layer is reported to attain a size reduction of more than 60% for multiple patch microstrip antennas [16]. This study is designed to present diverse two and four-element patch antennas at 2.5 GHz. It is noted that a narrow AMC bandwidth in designing broadband microwave technologies and antennas is a drastic drawback [19]. Therefore, there are few types of research for working on broadening the bandwidth of AMC structures [20]-[23]. Based on the frequency selective surface (FSS), an AMC design for RFID applications is proposed in [22]. In [23], a bandwidth of 4.4% at the resonance of 6.2 GHz is demonstrated to acquire a compact AMC unit cell with relatively acceptable angular stability.

In recent years, by increasing the extension of wireless networks and satellite applications, microstrip patch antennas have attracted a great deal of attention owing to their charming specifications, like a low-profile structure, light weight and simple implementation. Although a limited impedance bandwidth of the introduced antennas is accounted a notable issue in most studies. Diverse approaches in previous works have been developed to ameliorate the bandwidth of microstrip antennas [24]-[26]. Recently, by ameliorating the variety of integrated circuit technologies, the broadband AMC surfaces in the low-profile antennas and microwave devices are impressively utilized with the improved features [27]-[37]. In [29], a low profile circular polarized antenna with the AMC surfaces like a reflector plate is reported to provide a broadband antenna with a higher gain. This antenna with AMC

includes the impedance bandwidth from 1.19–2.37 GHz (66.3%) with the axial ratio AR bandwidth of 1.25–1.97 GHz (44.7%).

The present study reports a detailed discussion of the new broadband AMC design for applying at the suggested PSA. At first, a planar AMC is introduced to resonate at 10.14 GHz (8-12.35 GHz) for broadband application. In the following, a low-profile broadband PSA backed by the planar AMC surface is introduced. For this purpose, two radiating tapered slots fed by CPW broaden the impedance bandwidth in X-band. Then, a broadband 9×9 planar AMC reflector is developed under the antenna to obtain the ameliorated radiation efficiency. It presents the measured -10 dB impedance bandwidth in 6.63-13.73 GHz with the measured bandwidth of 70%. Also, the proper impedance matching and broad bandwidth with excellent compactness are achieved. Meanwhile, the performance of the AMC surface inserted in PSA is studied by investigating different AMC surfaces.

II. SUGGESTED PRINTED TAPERED SLOT ANTENNA WITH BROADBAND AMC SURFACE

3D view and top view of suggested PSA backed by planar AMC surface is drawn in Fig. 1. Two radiating slots with tapered slots are placed on FR4 substrate with 1.6 mm thickness. The 9×9 periodic patch of AMC surface is placed underneath the ground plane which is made from substrate thickness (FR4) of h_1 *to* couple the energy to the top layer of PSA. The dimensions of width and length of slots with tapered slots are 22 mm, and they etch on the substrate by sizes of 75×78 mm^2. The CPW feeding system of PSA for 50-Ω input impedance is utilized. The main design parameters select as thickness h_1=2.4 mm, and h_2=1.6 mm, ε_r=4.4 and tanδ=0.02 for FR4 substrates. A 50-Ω CPW feed is employed with the width of the strip 3 mm and the width of the slot 0.3 mm to provide the optimum impedance matching. Also, the value of L_{cpw}=23.5 mm for CPW length is optimized. The arrangement of the 9×9 AMC periodic ground plane is developed below the PSA as the reactive coupling to conclude a broader bandwidth.

The suggested antenna excites by a 50-Ohm SMA connector from the center of the structure. The parametric studies are employed to determine the optimum dimensions and slots' length. The sizes of the suggested structure with AMC are listed in Table I. The Images of the fabricated cases of the PSA backed by the planar AMC reflector are shown in Fig. 2.

The proposed PSA is introduced based on tapered slots for achieving different resonances [4]. The length, width and position of slots into the tapered slot patch result in a broad bandwidth. By incorporating two slots into the patches with tapered shapes, various resonances occur and thus the impedance bandwidth can be broadened.

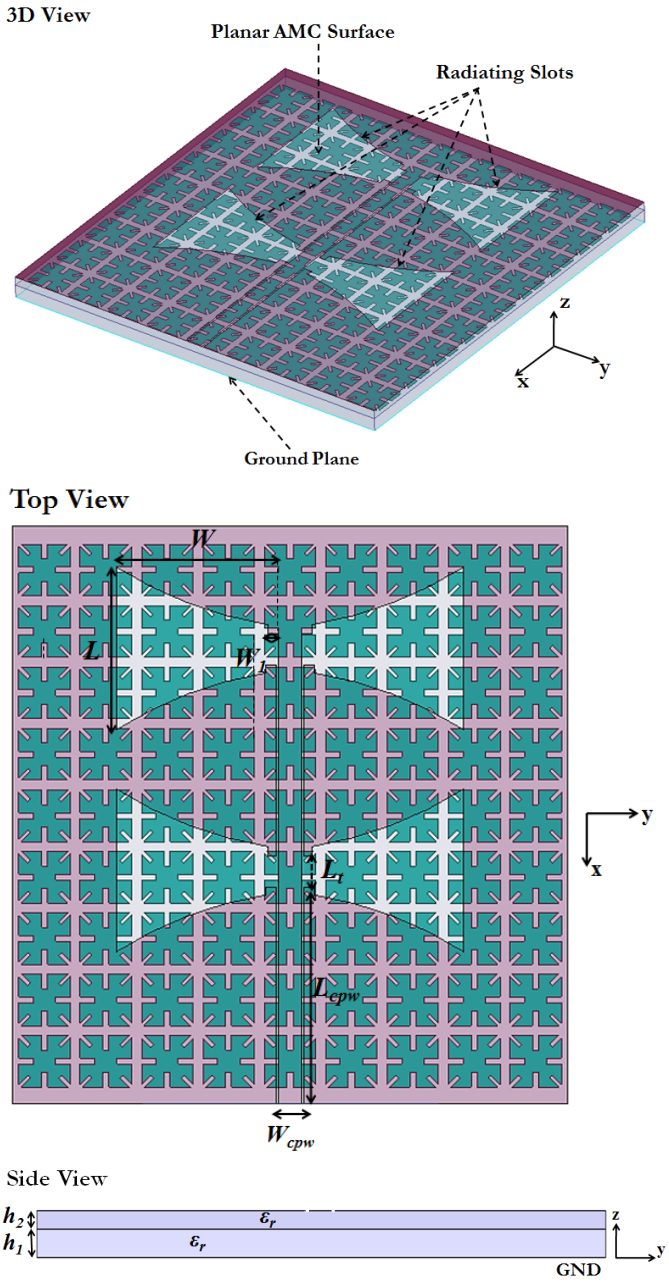

FIGURE 1. Structure of the suggested PSA backed by the broadband planar AMC reflector.

The conventional microstrip patch antenna is modelled as a simple resonant circuit L_1C_1, as seen in the Fig. 2 (a) with the presented lumped elements [3]:

$$C_1 = \frac{\varepsilon_e \varepsilon_0 L_e W}{2h} \cos^{-2}\left(\frac{\pi y_0}{L}\right) \quad (1)$$

$$L_1 = \frac{1}{(2\pi f_r)^2 C_1} \quad (2)$$

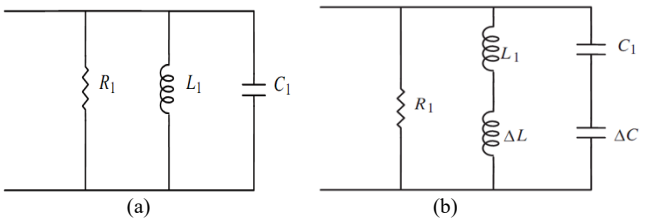

FIGURE. 2. (a) Equivalent circuit for simple patch (b) Equivalent circuit for PSA with tapered slots.

$$R_1 = \frac{Q}{\omega C_1} \tag{3}$$

$$Q = \frac{c\sqrt{\varepsilon_e}}{4 f_r h} \tag{4}$$

where y_0, L_e, f_r, h and ε_e are the distance of feed point from the edge, the effective length of the patch, the frequency of operating band and substrate characteristics, respectively. When two slots incorporate into the patch as a taper, an additional series inductance ΔL and an additional capacitance ΔC can be modelled as shown in Fig. 2 (b). Thus, different inductive and capacitive couplings in the proposed PSA design result in the wide impedance bandwidth with multiple resonances.

On the Basis of the transmission line model for the rectangular radiating patch, the basic width (W) and length (L) of the patch at the resonant frequency are determined using equations (5)-(8) [26]:

$$W = \frac{\lambda_0}{2\sqrt{\frac{\varepsilon_r + 1}{2}}} \tag{5}$$

$$L = \frac{c}{\quad} - 2\Delta L \tag{6}$$

$$\varepsilon_{eff} = \frac{\varepsilon_r + 1}{2} + \frac{\varepsilon_r - 1}{2}\left(\frac{1}{\sqrt{1 + 12\frac{h}{W}}}\right) \tag{7}$$

$$\Delta L = 0.412h\left(\frac{\left(\varepsilon_{eff} + 0.3\right)\left(\frac{W}{h} + 0.264\right)}{\left(\varepsilon_{eff} - 0.258\right)\left(\frac{W}{h} + 0.813\right)}\right) \tag{8}$$

Where, ε_{eff}, h and ΔL are effective permittivity coefficient, thickness and additional length due to fringing fields, respectively. Similarly, the basic width and length of printed microstrip dipole antenna are designed based on the equations (5)-(8) for determined operating frequency at X-band. In this case, dielectric constant substrate, ε_r=4.4 is considered. The optimum sizes of the proposed PSA such as different lengths and total height of the patch are optimized by full-wave simulator with the parametric study.

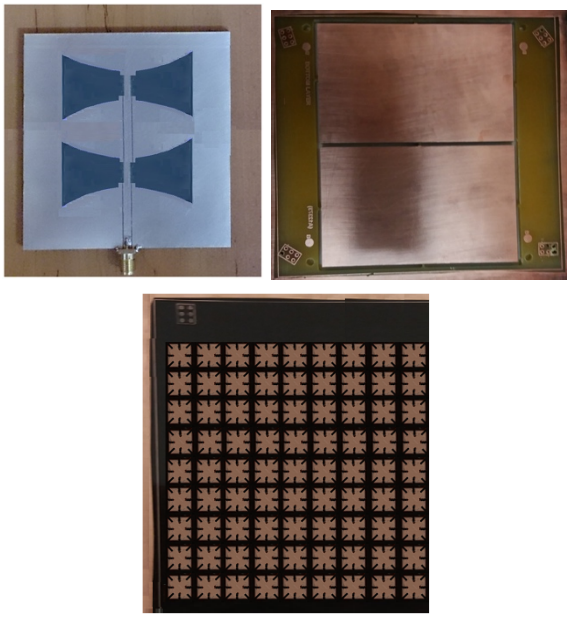

FIGURE. 3. Images of fabricated cases of the PSA backed by the planar AMC reflector.

Table I: Sizes of suggested PSA backed by the AMC

Parameters	Values (mm)
W	22
W_1	1.5
L	22
L_t	4.3
L_{cpw}	23.5
W_{cpw}	3
h_1	2.4
h_2	1.6
m	0.5
l	6.3
n	1.75
k	0.8
p	2.75

The arrangement of the 9×9 AMC periodic ground plane is developed below the PDA as the reactive coupling to conclude a broader bandwidth and enhancement of radiation properties. The parametric studies are employed in the full-wave simulator to determine the optimum dimensions and arms' length.

Fig. 5 demonstrates the geometry of a suggested rhomboid AMC unit cell. The regular patches are combined with different slots. The relative permittivity and thickness of ε_r=4.4 and h=2.4 mm, respectively are selected to realize on an FR4 substrate. The dimension of the unit cell equal to 7.3×7.3 mm^2 and the size of the ground plane is selected 8.3×8.3 mm^2. The electrical and structural specifications of the rhomboid AMC are the main factors on obtaining the enhanced bandwidth. The structural specification of the broad AMC bandwidth acquires from the reactance couplings for arms, slots and parasitic patches. The optimum AMC bandwidth is gained by choosing the suitable electrical specification as h and ε_r. Based on this, the angular stability should remain without variation for broadband applications. Indeed, various parts with slots

insert into the rhomboid AMC design, lead to an extra inductance and capacitance and an extensive AMC bandwidth is obtained [26].

The mushroom-type EBG structure is formed by a via-loaded metal patch which can be characterized by an equivalent parallel *LC* resonator with a resonant frequency $f_r=1/(2\pi\sqrt{LC})$. The inductance L is obtained by the current path between the patch surface and ground plane through via. Besides, the capacitance C represents the gap effect between two adjacent patches (see Fig. 4 (b)). The values of *LC* resonator and the frequency band gap in terms of the EBG parameters can be determined by the following formulas [11]:

$$C = \frac{W_{ebg}\varepsilon_0(1+\varepsilon_r)}{\pi}\cosh^{-1}\left(\frac{2W_{ebg}+g}{g}\right) \tag{9}$$

$$L = \mu_0 h \tag{10}$$

$$BW = \frac{1}{\eta}\sqrt{\frac{L}{C}} \tag{11}$$

where, ε_0, μ_0, W_{ebg}, and g are the permittivity and permeability of free space, patch width and gap between unit cells respectively. Also, η is the free space impedance which is 120π.

The electromagnetic properties of the suggested AMC are analyzed based on the finite element method (FEM) for periodic arrangements. As shown in Fig. 4 (a), an infinite model is fulfilled with a periodic boundary condition (PBC) at the surrounding faces. For this purpose, different scan angles of incident waves (θ) are performed to recognize a wideband performance with angular stability for reflection phase (see Fig. 4 (a)) at operating band. Moreover, the infinite model by applying Floquet port helps to determine the operational bandwidth of AMC at a given ±90˚ reflection phase.

According to Fig. 5, the flow chart of the design process is introduced in the different steps. It shows the comprehensive model to attain an optimum proposed design for wideband performance.

III. EXPERIMENTAL AND SIMULATION RESULTS WITH DISCUSSIONS

An investigation of reflection responses of the periodic AMC is discussed in this section. Also, the printed slot antenna backed by the planar AMC surface is tested to achieve low profile broadband antenna.

A. Infinite AMC Unit Cell with Simulation Results

The finite element method based on the Floquet theory is utilized in Ansoft High-Frequency Structure Simulator (HFSS) to simulate the AMC designs. Fig. 6 plots the reflection phase of the suggested AMC by radiating the

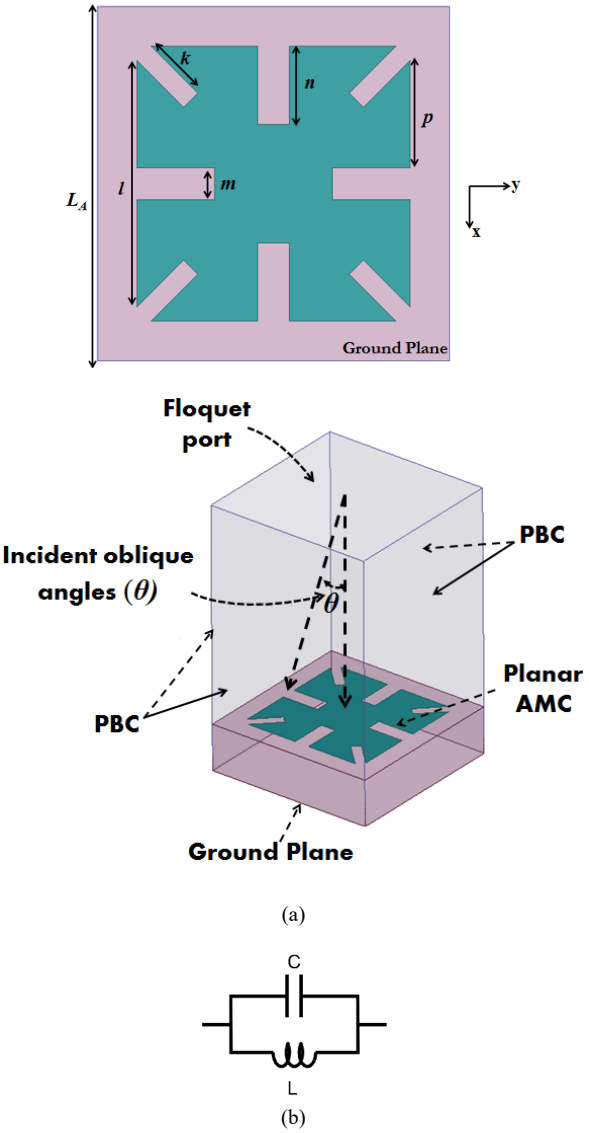

FIGURE. 4. (a) Structure of suggested planar design and simulation box by using Floquet theory (b) equivalent circuit model.

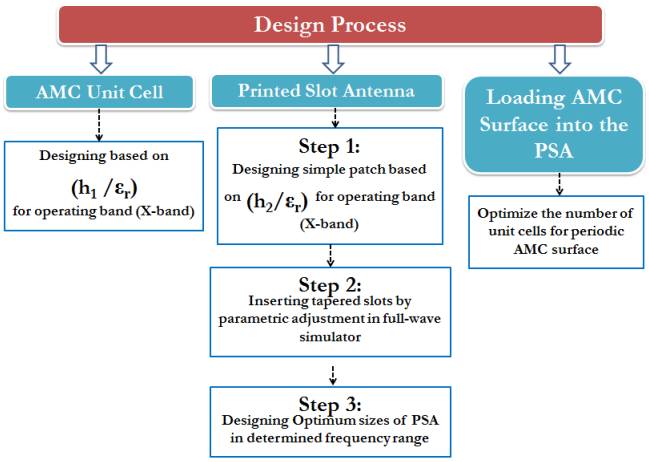

FIGURE. 5. Flow chart of the design process for the proposed structure.

perpendicular TE/TM waves. The frequency range for reflection phases between +90˚ to −90˚ is ordinarily considered as an AMC operation bandwidth [11]:

$$BW_{AMC}(\%) = [(f_{up} - f_{lo})/ f_c] \times 100 \quad (12)$$

where, f_{up} is the frequency at which reflection phase equals -90˚, f_{lo} is the frequency at which reflection phase equals +90˚, and f_c is the center frequency where reflection phase equals 0˚.

The simulated result of 8-12.35 GHz (43.1%) for normal TE/TM waves is provided. This AMC resonates at resonances of 10.14 GHz. As compared to the known research [11], [20]-[23], the suggested AMC expresses the acceptable characteristics. It indicates the symmetric unit cell design with the same response for TE/TM waves, considerably broader bandwidth and tuning ability of the significant factors to gain diverse outputs for broadband application. Fig. 6 plots the reflection phases of the planar AMC for diverse inclined incident waves (θ) from 0˚ to 60˚ in two polarization angles of φ=0˚ and 90˚. A good agreement between the outcomes of TE and TM waves is identified. Thus, it can be concluded that the planar AMC design covers X-band for wideband operation.

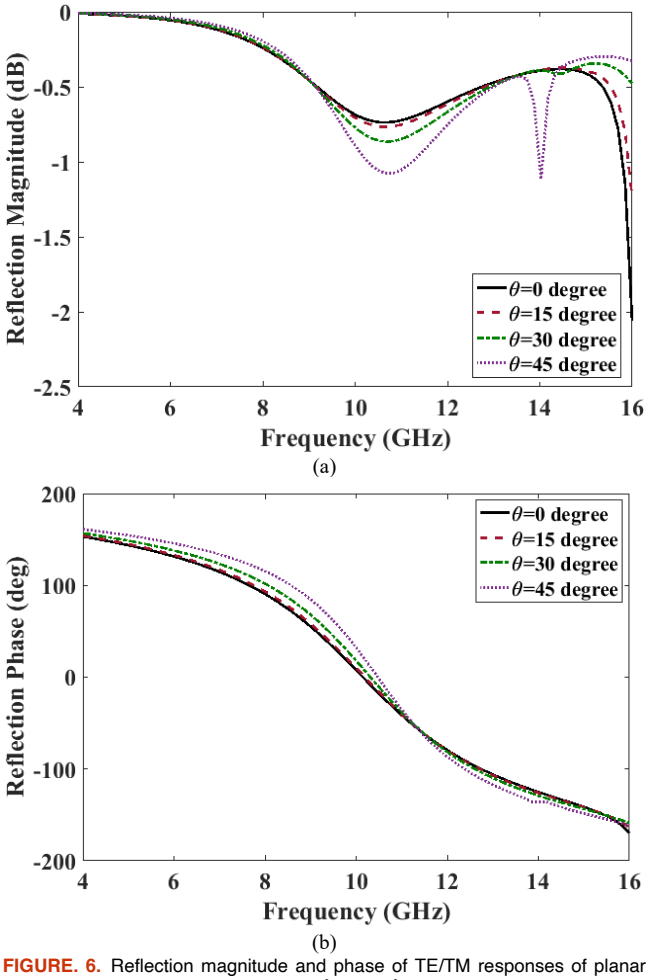

FIGURE. 6. Reflection magnitude and phase of TE/TM responses of planar AMC for indirect incident waves in ϕ=0˚ and 90˚.

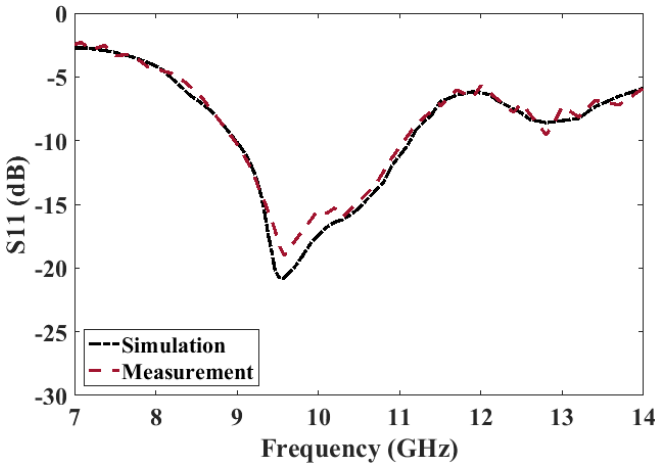

FIGURE. 7. Measurement and simulation results of S-parameters of the suggested PSA without AMC.

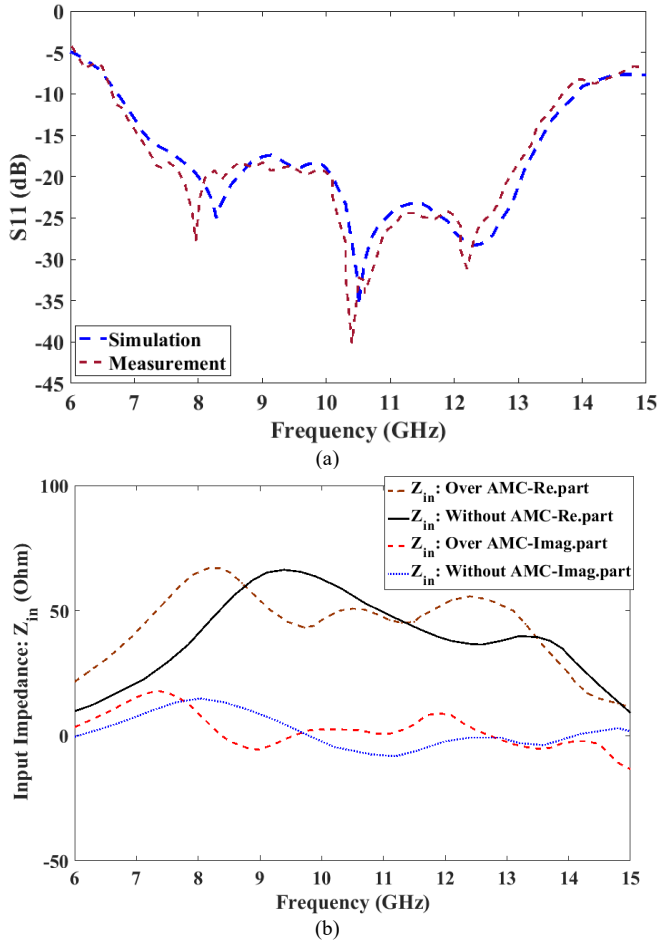

FIGURE 8. (a) Measurement and simulation results of S-parameters of the suggested PSA with planar AMC (b) Simulated input impedance results of proposed antenna.

B. Measurement And Simulation Results Of Printed Slot Antenna Loaded With AMC Surface

The measured and simulated S-parameters of the suggested PSA design without AMC are illustrated in Fig. 7. The PSA without AMC surface includes the measurement range of 9-11 GHz (20%) for S_{11}<-10 dB. As

seen from Fig. 8, the suggested antenna with the planar AMC reflector indicates the -10 dB measured bandwidth of 70% in 6.63-13.73 GHz. It is concluded that the PSA with the 9×9 AMC reflector presents the bandwidth enhancement of 50% versus the PSA without the AMC reflector. On the other hand, the decrease in frequency leads to suitable miniaturization.

Fig. 8 (b) shows the comparison between the input impedance curves of the proposed antenna with and without AMC. It indicates the operating modes of 8.25, 10.5 and 12.35 GHz for proposed design with AMC.

The total dimensions of the PSA without AMC reflector are $2.25\lambda_L$, $2.34\lambda_L$ and $0.048\lambda_L$, respectively (λ_L is the wavelength at the lower frequency). Whereas the total dimensions of the PSA with the planar AMC surface are $1.65\lambda_L$, $1.72\lambda_L$ and $0.088\lambda_L$, respectively. It is clear that by utilizing AMC the operating frequency of antenna reduce to the lower frequencies and consequently, a compact antenna with the reduced size is achieved. Thus, by introducing the planar AMC reflector in the suggested PSA size reduction of 60% gains compared with the PSA without the AMC. As an interesting note, at the PSA with the AMC reflector a minimum impedance matching of almost -40 dB occurs over the obtained bandwidth. The suggested PSA with the AMC reflector in comparison with the PSA without AMC has excellent matching.

Fig. 9 plots the surface current density on the patch of the printed antenna and AMC surfaces at various resonant frequencies. As seen from Figs. 9 (a) at the lower resonance of 8.3 GHz of suggested design with planar AMC, a current distribution dominates on the CPW feed line and the sections of the AMC unit cells that are located under the CPW feed line. It is obtained that in Fig. 9 (b) at the higher resonance of 12.2 GHz, the current density distributes on most unit cells of the AMC and around the tapered slots.

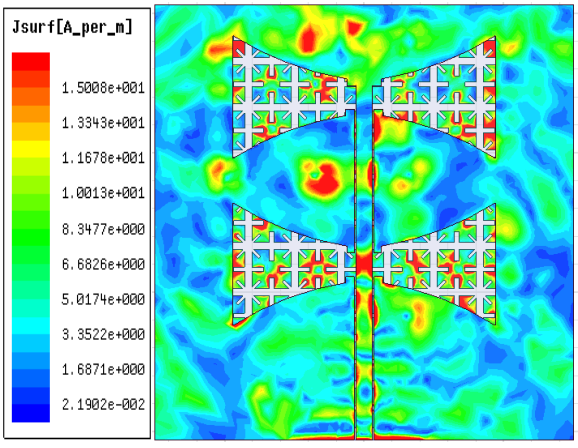

(a)

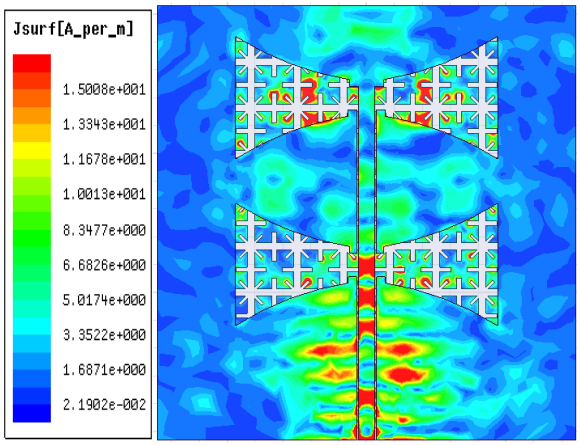

(b)

FIGURE. 9. Surface current density on the patch of the proposed antenna with planar AMC at: (a) 8.3 (b) 12.2 GHz.

The measurement and simulation results of radiation patterns in the xz-plane and yz-plane for the suggested PSA with the planar AMC reflector are plotted in Fig. 10. It is well found out that suitable accordance of the results is appointed. Simultaneously, the suggested design presents acceptable unidirectional radiation patterns. The maximum gain of the suggested PSA with planar AMC surface within the operational bandwidth is 11.1 dBi, as seen in Fig. 11. Thus, the gain of the structure is impressively increased over obtained impedance bandwidth compared to the antenna without AMC.

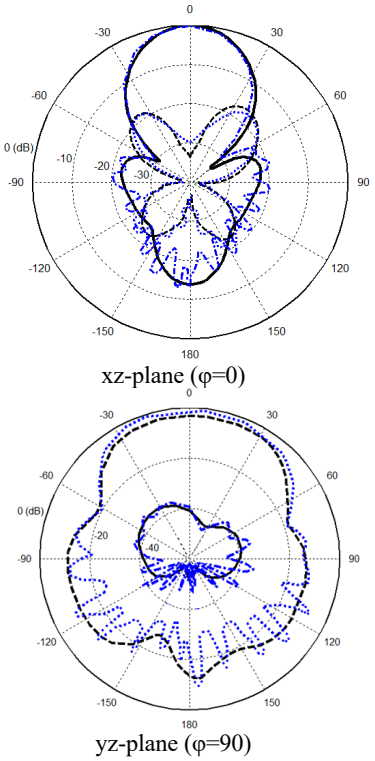

xz-plane (φ=0)

yz-plane (φ=90)

(a)

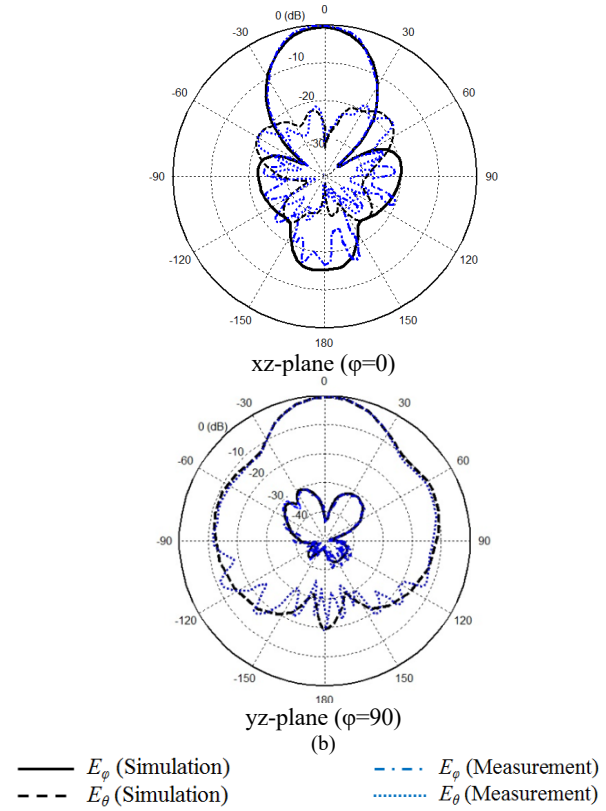

FIGURE. 10. Measurement and simulation results of radiation patterns of the suggested PSA with the planar AMC surface for co and cross-polarization (a) 8.3 GHz (b) 12.2 GHz.

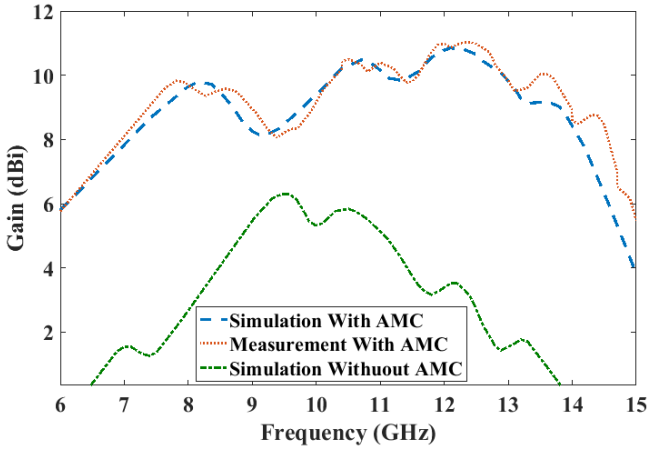

FIGURE. 11. Simulated and measured gain of the suggested design with and without AMC surface.

As seen in Fig. 12, the good results of the proposed design for the measured and simulated radiation efficiencies are achieved.

The comparative behavior of the proposed design is depicted in Table II. It well presents the remarkable features of the suggested structure which includes considerable size reduction, wider bandwidth and enhanced maximum gain. The suggested design compared with the previous research works with planar AMCs like [31]-[34] introduces a broader bandwidth with more size reduction and enhanced impedance matching over the operating bandwidth.

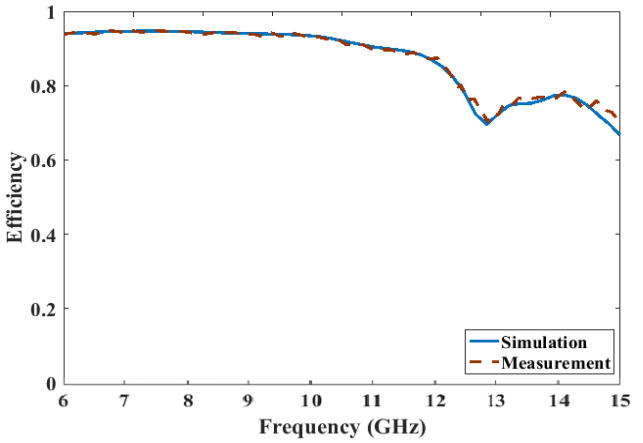

FIGURE. 12. Simulated and measured efficiency of the suggested design with AMC surface.

The proposed structure is considered a following design process to show an acceptable performance:

- Suggesting a wideband AMC design in 8-12.35 GHz (43.1%) for X-band operation and investigation of their properties in the infinite condition.
- Designing a broadband printed slot antenna using tapered slots fed by CPW in X-band (9-11 GHz).
- Designing a low profile printed antenna loaded with the planar AMC surface for wideband applications with improved radiation performance.

For this purpose, the suggested design compared with the previous research works with planar AMCs like [6], [19], [20], [29], and [31]-[37] introduces a broader bandwidth of 70% and a higher gain of 11.1 dBi with enhanced impedance matching over the operating bandwidth until -40 dB. For example, a proposed MIMO array in [19] with the size of 75×75×12.7 mm^3 indicates a wide bandwidth of 3-4.1 GHz and maximum gain of 7.1 dBi. Also, a reported array with EBG in [37] introduces a bandwidth of 8-9.25 GHz (14.5%) with 96×96×1.6 mm^3 and high gain of 7 dBi. Thus, it can be concluded that the proposed design introduces a compact wideband antenna with enhanced gain for X-band operation.

The performance of the planar AMC surface developed in PSA is studied by applying various periodic AMC unit cells. Based on the simulated reflection results of the proposed structures in Fig. 13, the optimal AMC reflector is determined.

At the same time, to recognize the number of unit cells in the reflector, the reflection properties of four planar AMC surfaces are studied. The features of four AMC surfaces are analyzed (See Fig. 13): (a) Design#1; 7×9 AMC reflector, (b) Design#2; 9×7 AMC reflector, and (c) Design#3; 9×9 AMC reflector.

The simulated S-parameters of the suggested design with different planar AMC surfaces in Fig. 13 are plotted in Fig. 14. It confirms the introduced method of the equivalent waveguide feed to recognize the optimal numbers of unit cells in the proposed structure. According to the results, the optimum Design#3 leads to wideband performance with better impedance matching.

Table II. Comparison of suggested designs with other studies

Proposed design	Bandwidth Without AMC	Bandwidth With AMC and impedance matching	Size of antenna (Width×Length×Height)	Maximum Gain
Suggested PSA with planar AMC	9-11 GHz (20%)	6.63-13.73 GHz (70%) Minimum Matching: -40 dB	75×78×4 mm^3	11.1 dBi
Bow-tie antenna with AMC in [33]	1.67-2.06 GHz	1.64-1.94 GHz (16.8%) Minimum Matching: -25 dB	50×70×25 mm^3	6.5 dBi
antenna with AMC in [34]	7.25-7.75 GHz	6.9–7.9 GHz (13.5%) Minimum Matching: -25 dB	76×76×7 mm^3	13 dBi
Bowtie dipole antenna with AMC in [19]	3.1-3.9 GHz	3–4.1 GHz (31%) Minimum Matching: -30 dB	75×75×12.7 mm^3	7.1 dBi
antenna with AMC in [31]	2.06-2.89 GHz	1.83-2.72 GHz (39%) Minimum Matching: -23 dB	120×120×16 mm^3	6 dBi
antenna with AMC in [32]	5.2-6.5 GHz	4.8-6.6 GHz (32%) Minimum Matching: -23 dB	42×24×6.8 mm^3	7 dBi
antenna with EBG-MTM in [36]	9.45-9.75 GHz	8.7-11.7 GHz (29.4%), 11.9-14.6 GHz Minimum Matching: -40 dB	37×70×1.6 mm^3	9.15 dBi
2×2 array with EBG in [37]	8.4-8.78 GHz	8-9.25 GHz (14.5%) Minimum Matching: -15 dB	96×96×1.6 mm^3	7 dBi
antenna with AMC in [20]	9.65-9.70 GHz	5.80-6.1 GHz, 8.94-9.18 GHz (3%) Minimum Matching: -21 dB	64×64×1.6 mm^3	7.9 dBi
antenna with AMC in [6]	8.25-8.45 GHz	6.98-8.57 GHz (20.4%) Minimum Matching: -31 dB	68×68×33.6 mm^3	9.3 dBi

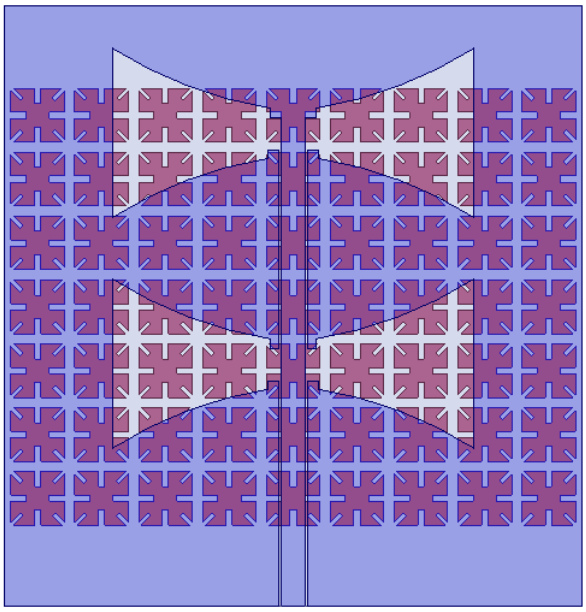

(a)

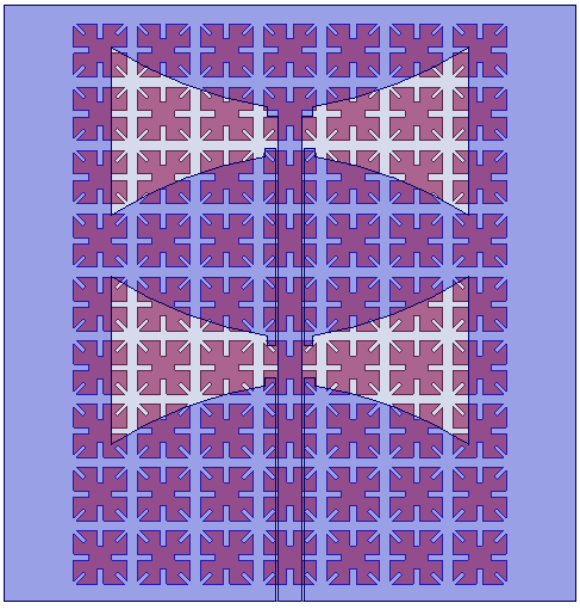

(b)

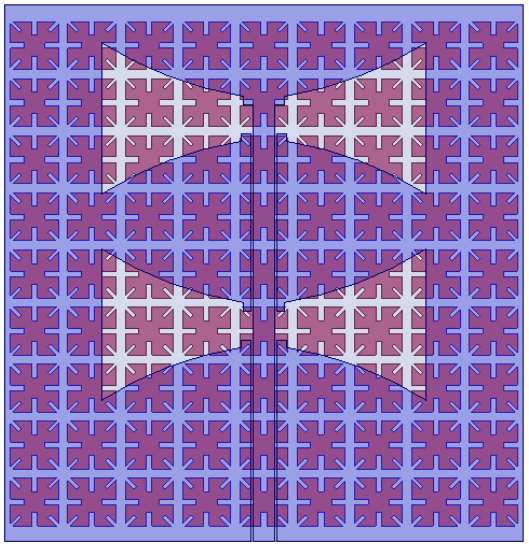

(c)

FIGURE. 13. Three different rhomboid AMC reflectors used in suggested PSA; (a) Design#1: 7×9 AMC surface, (b) Design#2: 9×7 AMC surface, (c) Design#3: 9×9 AMC surface (main case).

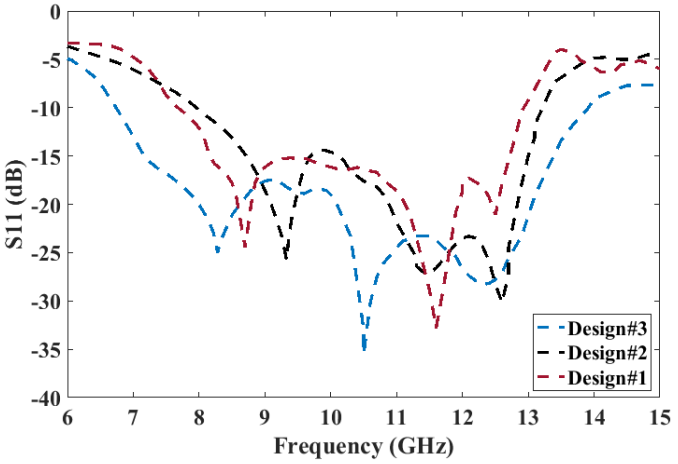

FIGURE. 14. S-parameters of the suggested design for different AMC unit cells.

IV. CONCLUSION

The novel design of the planar AMC unit cell is introduced to provide a broadband response, in this study to include 8-12.35 GHz (43.1%). The introduced AMC indicates distinguished properties with proper stability within the AMC bandwidth. It is verified that the planar AMC is helpful in broadband applications by investigating the reflection responses at the different polarization angles for diverse incident waves. The suggested PSA with tapered slots backed by 9×9 AMC reflector introduces the low profile broadband structure for X-band operation. By adding planar AMC surface into the PSA the -10 dB impedance bandwidth of 6.63-13.73 GHz is achieved. The proper impedance matching until -40 dB, excellent compactness and broader bandwidth were obtained from the suggested PSA with AMC compared with the PSA without AMC. Besides, the uni-directional radiation patterns with a high gain are achieved. From experimental results, the acceptable efficiency is reported, and it is concluded that the suggested design can be used for broadband systems. Finally, the performance of the AMC reflector inserted in the PSA is studied by investigating three cases of AMC surfaces. In this regard, the optimum number of AMC patches is given for broadband operation.

REFERENCES

1. Z. Wang, Y. Sun, J. Yang, Y. Zhang , "Interferograms of Votex FWM Beam for Nonlinear Spatial Filter in Photonic Band Gap," *IEEE Photonics Journal.,* vol. 11, no. 1, pp. 1854–1859, 2019.
2. A. A. Roseline, K. Malathi, A. K. Shrivastav, "Enhanced performance of a patch antenna using spiral-shaped electromagnetic bandgap structures for high-speed wireless networks," *IET Microw. Antennas Propag.,* vol. 5, no. 14, pp. 1750–1755, 2011.
3. A. Foroozesh, and L. Shafai, "Investigation Into the Application of Artificial Magnetic Conductors to Bandwidth Broadening, Gain Enhancement and Beam Shaping of Low Profile and Conventional Monopole Antennas," *IEEE Trans. Antennas Propag*., vol. 59, no. 1, pp. 4–20, 2011.
4. S. Jam and H. Malekpoor, "Compact 1×4 patch antenna array by means of EBG structures with enhanced bandwidth", *Microw. Opt. Technol. Lett,* vol. 58, no. 12, pp. 2983-2989, 2016.
5. A. Foroozesh, and L. Shafai, "Effects of artificial magnetic conductors in the design of low-profile high-gain planar antennas with high-permittivity dielectric superstrate," *IEEE Antennas Wireless Propag. Lett.,* vol. 8, pp. 10-13, 2009.
6. H. Malekpoor, A. Abolmasoumi, and M. Hamidkhani, "High gain, high isolation, and low-profile two-element MIMO array loaded by the Giuseppe Peano AMC reflector for wireless communication systems," *IET Microw. Antennas Propag.,* vol. 16, Is. 1, pp. 46–61, 2022.
7. S. Rajagopal, G. Chennakesavan, D. R. P. Subburaj, R. Srinivasan, and A. Varadhan, "A dual polarized antenna on a novel broadband multilayer Artificial Magnetic Conductor backed surface for LTE/CDMA/GSM base station applications," *AEU- Int. J. Electron. Commun.,* vol. 80, pp. 73–79, 2017.
8. J. M. Bell, M. F. Iskander, and J. J. Lee, "Ultrawideband hybrid EBG/ferrite ground plane for low-profile array antennas," *IEEE Trans. Antennas Propag.,* vol. 55, no. 1, pp. 4–12, 2007.
9. D. Nashaat, H. A. Elsadek, E. A. Abdallah, M. F. Iskander, and H. M. E. Hennawy, "Ultrawide bandwidth 2×2 microstrip patch array antenna using electromagnetic band-gap structure (EBG)," *IEEE Trans. Antennas Propag.,* vol. 59, no. 5, pp. 1528–1534, 2011.
10. S. Barth, and A. K. Iyer, "A Miniaturized Uniplanar Metamaterial-Based EBG for Parallel-Plate Mode Suppression," *IEEE Trans. Microw. Theory Tech.,* vol. 64, no. 4, pp. 1176–1185, 2016.
11. D. Sievenpiper, L. Zhang, R. F. J. Broas, N. G. Alex´opolous, and E. Yablonovitch, "High-impedance electromagnetic surfaces with a forbidden frequency band," *IEEE Trans. Microw. Theory Tech.,* vol. 47, no. 11, pp. 2059–2074, 1999.
12. J. Y. Deng, J. Y. Li, L. Zhao, L. X. Guo, "A Dual-Band Inverted-F MIMO Antenna With Enhanced Isolation for WLAN Applications ," *IEEE Antennas Wireless Propag. Lett.,* vol. 6, pp. 2270 - 2273, 2017.
13. H. Malekpoor and M. Hamidkhani, "Performance Enhancement of Low-Profile Wideband Multi-Element MIMO Arrays Backed by AMC Surface for Vehicular Wireless Communications," *IEEE ACCESS*, vol. 9, pp. 166206 - 166222, 2021.

14. H. Lee, B. Lee, "Compact Broadband Dual-Polarized Antenna for Indoor MIMO Wireless Communication Systems," *IEEE Trans. Antennas Propag.,* vol. 64, pp. 766 - 770, 2016.
15. E. Ameri, S. H. Esmaeli, and S. H. Sedighy, "Wide band radar cross section reduction by thin AMC structure," *AEU- Int. J. Electron. Commun.,* vol. 93, pp. 150–153, 2018.
16. S. Ghosh, T. N. Tran, T. L. Ngoc, "Dual-Layer EBG Based Miniaturized Multi-Element Antenna for MIMO Systems," *IEEE Trans. Antennas Propag.,* vol. 62, no. 8, pp. 3985 - 3997, 2014.
17. X. Y. Liu, Y. H. Di, H. Liu, Z. Wu, and M. M. Tentzeris, "A Planar Windmill-like Broadband Antenna Equipped with Artificial Magnetic Conductor for Off-Body Communications," *IEEE Antennas Wireless Propag. Lett.,* vol. 15, pp. 64 - 67, 2015.
18. H. Malekpoor , "Comparative investigation of reflection and band gap properties of finite periodic wideband artificial magnetic conductor surfaces for microwave circuits applications in X-band," *International Journal of RF and Microwave Computer-Aided Engineering*., vol. 29, Is. 10, pp. 1–13, 2019.
19. J. Zhu, S. Li, S. Liao; Q. Xue, "Wideband Low-Profile Highly Isolated MIMO Antenna with Artificial Magnetic Conductor," *IEEE Antennas Wireless Propag. Lett.,* vol. 17 pp. 458 - 462, 2018.
20. A. Ghosh, V. Kumar, G. Sen, S. Das, "Gain enhancement of triple-band patch antenna by using triple-band artificial magnetic conductor," *IET Microw. Antennas Propag.*, vol. 12, no. 8, pp. 1400-1406, 2018.
21. N. Othman, N. A. Samsuri, M. Ka. A. Rahim, and K. Kamardin, "Low specific absorption rate and gain-enhanced meandered bowtie antenna utilizing flexible dipole-like artificial magnetic conductor for medical application at 2.4 GHz," *Microw Optical. Tech Lett.,* vol. 62, pp. 3881-3889, 2020.
22. M. E. de Cos, Y. Álvarez, and F. L. Heras, "Planar artificial magnetic conductor: design and characterization setup in the RFID SHF band," *IEEE Antennas Wireless Propag. Lett.,* vol. 23, pp. 1467–1478, 2009.
23. R. C. Hadarig, M. E. de Cos and F. L. Heras, "Novel miniaturized artificial magnetic conductor," *IEEE Antennas Wireless Propag. Lett.,* vol. 12, pp. 174–177, 2013.
24. H Malekpoor, and M. Shahraki "Radiation Properties Improvement of 1 × 4 Array of Wideband Printed Antenna Supported by AMC Surface for Vehicular MIMO Systems," *Radio Science,* vol. 57, pp. 1–18, 2022.
25. X. Yang, L. Ge, J. Wang, C. Y. D. Sim, "A Differentially Driven Dual-Polarized High-Gain Planar Patch Antenna," *IEEE Antennas Wireless Propag.* vol. 17, pp. 1181 - 1185, 2018.
26. K. D. Xu, H. Xu, Y. Liu, J. Li, Q. H. Liu, "Microstrip Patch Antennas With Multiple Parasitic Patches and Shorting Vias for Bandwidth Enhancement," *IEEE Access.,* vol. 6, pp. 11624 - 11633, 2018.
27. Z. Xu, and C. Deng, "High-Isolated MIMO Antenna Design Based on Pattern Diversity for 5G Mobile Terminals," *IEEE Antennas Wireless Propag. Lett.,* vol. 19 pp. 467 - 471, 2020.
28. B. S. Cook and A. Shamim, "Flexible and compact AMC based antenna for telemedicine applications," *IEEE Trans. Antennas Propag.,* vol. 61, no. 2, pp. 524 - 531, 2013.
29. D. Feng, H. Zhai, L. Xi, S. Yang, K. Zhang, D. Yang, "A Broadband Low-Profile Circular-Polarized Antenna on an AMC Reflector," *IEEE Antennas Wireless Propag. Lett*., vol. 16, pp. 2840 - 2843, 2017.
30. S. Yan, P. J. Soh, M. Mercuri, D. M.M.-P. Schreurs, G. A. E. Vandenbosch, "Low profile dual-band antenna loaded with artificial magnetic conductor for indoor radar systems," *IET Microw. Antennas Propag.,* vol. 9, no. 2, pp. 184–190, 2015.
31. J. Liu, J. Y. Li, J. J. Yang, Y. X. Qi, R. Xu, "AMC-Loaded Low-Profile Circularly Polarized Reconfigurable Antenna Array," *IEEE Antennas Wireless Propag. Lett.*, vol. 19, pp. 1276 - 1280, 2020.
32. G. Li, H. Zhai, L. Li, C. Liang, R. Yu and S. Liu, "AMC-loaded wideband base station antenna for indoor access point in MIMO system," *IEEE Trans. Antennas Propag.,* vol. 63, no. 2, pp. 525–533, 2015.
33. Y. W. Zhong, G. M. Yang and L. R. Zhong, "Gain enhancement of bow-tie antenna using fractal wideband artificial magnetic conductor ground," *Electron. Lett.*, vol. 51, no. 4, pp. 315-317, 2015.
34. J. P. Turpin,, Q. Wu, D. H. Werner, B. Martin, M. Bray, and E. Lier, "Near-zero-index metamaterial lens combined with AMC metasurface for high-directivity low-profile antennas", *IEEE Trans. Antennas Propag*., vol. 62, (4), pp. 1928–1936, 2014.
35. J. Joubert, J. C. Vardaxoglou, W. G. Whittow, and J. W. Odendaal, "CPW-fed cavity-backed slot radiator loaded with an AMC reflector," *IEEE Trans. Antennas Propag.,* vol. 60, no. 2, pp. 735–742, 2012.
36. M. Alibakhshikenari, M. Khalily, B. S. Virdee, C. H. See, R. Abd-Alhameed, F. Falcone, and E. Limiti, "Mutual Coupling Suppression Between Two Closely Placed Microstrip Patches Using EM-Bandgap Metamaterial Fractal Loading", *IEEE Access*, vol. 7, pp. 23606 – 23614, March 5, 2019.
37. M. Alibakhshikenari, B. S. Virdee, C. H. See, R. Abd-Alhameed, A. H. Ali, F. Falcone, and E. Limiti, "Study on Isolation Improvement Between Closely Packed Patch Antenna Arrays Based on Fractal Metamaterial Electromagnetic Bandgap Structures", *IET Microw, Antennas & Propag.*, Vol. 12, Is. 14, 28 p. 2241 – 2247, 2018.